Neutral water splitting catalysis with a high FF triple junction polymer cell

Xavier Elias,[†1] Quan Liu,[†,1] Carolina Gimbert-Suriñach,[†,*,2] Roc Matheu,[2] Paola Mantilla-Perez,[1] Alberto Martinez-Otero,[1] Xavier Sala,[4] Jordi Martorell[*,1,3] and Antoni Llobet[*,2,4]

[1] ICFO-Institut de Ciencies Fotoniques, The Barcelona Institute of Science and Technology, 08860 Castelldefels (Barcelona), Spain

[2] Institute of Chemical Research of Catalonia (ICIQ), The Barcelona Institute of Science and Technology, Avinguda Països Catalans 16, 43007 Tarragona, Spain

[3] Departament de Física, Universitat Politècnica de Catalunya, Terrassa, Spain

[4] Departament de Química, Universitat Autònoma de Barcelona (UAB), 08193 Cerdanyola del Vallès, Barcelona, Spain

[*]Corresponding authors e-mail: cgimbert@iciq.es, jordi.martorell@icfo.es, allobet@iciq.cat

[†]These authors contributed equally to this work

The authors declare that they have no competing interests

Abstract

We report a photovoltaics-electrochemical (PV-EC) assembly based on a compact and easily processable triple homo-junction polymer cell with high fill factor (76%), optimized conversion efficiencies up to 8.7 % and enough potential for the energetically demanding water splitting reaction

(Voc = 2.1 V). A platinum-free cathode made of abundant materials is coupled to a ruthenium oxide on glassy carbon anode (GC-RuO_2) to perform the reaction at optimum potential (ΔE = 1.70-1.78 V, overpotential = 470-550 mV). The GC-RuO_2 anode contains a single monolayer of catalyst corresponding to a superficial concentration (Γ) of 0.15 nmol cm^{-2} and is highly active at pH 7. The PV-EC cell achieves solar to hydrogen conversion efficiencies (STH) ranging from 5.6 to 6.0 %. As a result of the solar cell's high fill factor, the optimal photovoltaic response is found at 1.70 V, the minimum potential at which the electrodes used perform the water splitting reaction. This allows generating hydrogen at efficiencies that would be very similar (96%) to those obtained as if the system were to be operating at 1.23 V, the thermodynamic potential threshold for the water splitting reaction.

Key words:

Water splitting, neutral pH, triple junction cell, OPV, GC-RuO_2 anode

1-Introduction

Among all renewable energies, photovoltaics (PVs) is the most easily integrable[1,2,3] in an urban environment where most of the electricity consumption occurs and where the energy distribution system is the largest. However, electricity production from sunlight is intermittent and does not always match the consumption pattern. It has been proposed that an optimal solution to perfectly combine photovoltaic integrability with a variable energy demand is to use the excess electricity produced during peak irradiation to drive the water splitting reaction to generate hydrogen fuel, so that the energy is stored in the form of chemical bonds.[4] Such energy production would have a close to negligible environmental impact while its distribution could be carried out effectively with the already existing natural gas pipelines. Unfortunately, at

present there are no PV hydrogen production systems that may offer integrability, low cost, durability and a high efficiency in one.

Different PV approaches using either multi-junction or series connected cells have been proposed to overcome the high thermodynamic potential of ΔE^o = 1.23 V of the water oxidation reaction.[5,6,7,8,9,10,11,12,13,14,15,16,17,18,19] Over-potentials associated with the reaction kinetics raise the required voltage by several hundreds of mV to 1.5 V or higher. Early examples used multiple junction silicon solar cells coupled to noble metal electrodes like platinum.[5-7,] Although high solar to hydrogen (STH) conversion efficiencies were achieved, the prohibitive costs of both the solar cells and the metal catalysts hampered the implementation of a large scale hydrogen generation. Recent approaches have replaced the expensive silicon triple junctions by metallic chalcogenide materials,[10] perovskites,[14-16] dye-sensitized,[17,18] or polymer[18] solar cells. However, either harsh alkaline, pH=14 in the majority of them, or acidic conditions were used to minimize the overpotentials and increase the STH efficiency of the system. The corrosion associated to such harsh conditions prevents a practical large scale hydrogen production using ocean or river water which is found close to a neutral pH.

In here, for an optimal water splitting reaction minimizing the overpotential limitation, we implemented a photovoltaic-electrochemical (PV-EC) system using a one-blend polymer triple junction cell which exhibits a high fill factor (FF) overcoming the FF of the single junction counter parts. This implies that at the lowest measured water splitting voltage of 1.70 V, the STH conversion efficiency under 1 sun AM1.5G illumination is as high as 96 % of the maximum efficiency possible corresponding to an ideal operation at the thermodynamic potential threshold. This is combined with the use of platinum free anode and cathode electrodes immersed in a water solution buffered at pH 7. A glassy carbon rod with an

extremely small amount of RuO_2 catalyst anchored on the graphite surface was used as anode (GC-RuO_2). In such GC-RuO_2 electrode configuration a strong catalytic activity for water oxidation is achieved at pH 7 with an amount of Ru that is at least 100 times smaller than the Ru found in commonly used RuO_x electrodes.[8,18b,20,21,22,23] Such a strong catalytic activity results from an optimum electrode surface morphology that consists of a monolayer of fully active material where all the available catalytic sites are accessible for the water oxidation reaction. The preparation of the electrode is based on using a ruthenium molecular precursor[24,25] that interconverts into the final RuO_2 active species upon electrochemical treatment, details on the synthesis and characterization of this anode can be found in Ref. [25]. We demonstrate that a high STH conversion efficiency at pH 7 is possible when the triple junction cell and GC-RuO_2 anode are combined with a cathode made of earth abundant materials deposited on a stainless steel plate (SST-NiMoZn).[11,26,27] When the described system is compared to a Pt-anode and Pt-cathode electrode configuration, we obtain a 250 mV reduction in the overpotentials for operation at pH 7. The overall PV-EC system we implement uses compact devices, earth abundant materials or very small amounts of rare metals, operates at the pH water is found in nature and the stability of the PV device under 1 sun illumination is ensured when a proper encapsulation is applied.[28]

2-Results and Discussion

2.1-Optimal triple junction polymer solar cell

The open circuit voltage of a single junction polymer cell is not sufficient to overcome the potential barrier for the water splitting chemical reaction. To achieve a V_{oc} of 2.1 V we piled up three single junction cells of the same PTB7:$PC_{71}BM$ blend (Fig. 1a). This blend has been shown to exhibit one of the top single junctio[29] or homo-tandem[30,31] polymer cell performances.

By using the same blend in the three sub-cells we simplify the fabrication procedure while at the same time we ensure a homogenous electrical performance throughout the device. This resulted in FFs as high as 76%, significantly higher than the 71% averaged by the single junction counterparts. Such high FFs, essential to minimize the impact of the overpotentials in the water splitting reaction, are in correspondence to the use of very thin active blend layers combined with a light absorption shared by the three sub-cells. In the single junction counterpart recombination is larger given that full light absorption is carried out by just one single junction.

Reaching the optimal light harvesting in triple junction PV architectures with high number of layers can only be achieved by setting a target solution and implementing an inverse solving problem approach to reach that solution.[1] In particular, the cell fabricated in this work has a total of thirteen layers with the configuration indicated in Fig. 1a. In addition, a series connected triple junction device requires matching of the short-circuit currents of the three sub-cells. This current matching combined with the largest possible short circuit current is the solution targeted by our numerical approach based on the transfer matrix[32,33] to numerically compute the electrical field distribution and light absorption within each one of the cell layers. The optimal electrical field intensity profile and simulated EQEs for each one of the sub-cells in the triple junction device is shown in Fig. 1b and 1c, respectively. The electric field intensity shows maxima in the rear sub-cell for the near infrared wavelengths, in the middle sub-cell for the wavelength range between 500 and 600 nm, and in the front sub-cell for the near UV range (Fig. 1b). Such field distribution implies that absorption at shorter wavelengths is dominated by the front sub-cell, in the middle range of the visible spectrum is dominated by the middle sub-cell, and at the near infrared by the rear sub-cell. Such perfectly balanced light absorption distribution among the three cells is clearly seen in the simulated EQEs shown in Fig. 1c. Such

large differences in the EQE can be explained in part by the different thicknesses of the layers, but also because of the interference. As can be seen in Fig. 1b constructive interference of the incident and reflected waves tends to favor IR shifted absorption for the rear cell and UV shifted absorption for the front cell. In one of the architectures leading to such optimal light absorption, the PTB7:PC71BM layer thicknesses were determined to be 60 nm, 105 nm, and 110 nm for the front, middle, and rear sub-cells, respectively. These values were used to fabricate triple-junction devices with measured conversion efficiencies up to 8.7% under AM 1.5G illumination at 100 mW/cm^2 and V_{oc} equivalent to 2.1 V. A typical current density−voltage (J−V) curve of the triple junction cell is shown in Fig. 2, with its relevant parameters marked in red. The potential extracted at the maximum power point of the cell was close to 1.76 V, 530 mV higher than the thermodynamic potential for the water splitting reaction. The high fill factor of the solar cell used (76%) ensures that the water splitting efficiency loss due to the catalyst overpotential will be minimum as opposed to a single junction series connection of three cells of the same polymer type that would exhibit a smaller FF around 71% (Fig. S2), or alternative options where the V_{oc} of the configuration would be too large.[34]

2.2-Coupled GC-RuO_2 anode and SST-NiMoZn cathode for water splitting catalysis

With the aim of minimizing the cost of the final PV-EC device for ultimate applications, we used a cathode of NiMoZn[26,27] on stainless steel electrode (SST-NiMoZn) made of earth abundant materials and an anode made of RuO_2 on glassy carbon electrode (GC-RuO_2).[25] The selected GC-RuO_2 anode is particularly interesting because it has an extremely low catalyst loading with a superficial concentration (Γ) of 0.15 nmol cm^{-2} and a roughness factor (RF) of 1-2, consistent with one monolayer of active material (see supporting information). These values are much lower than those of commonly used RuO_x or IrO_x based electrodes, that are

usually prepared using electrochemical deposition from $RuCl_3$,[20,21] dropcasting of suspensions with post-annealing processes[23] or sputtering techniques.[21,23] These deposition methods give layers of RuO_2 with thickness from tens of nanometers (*e.g.* 70 nm in ref 21) up to a few micrometers (*e.g.* 2.3 μm in ref 22). By using the molecular catalyst precursor methodology[25] we have a full control of the starting monolayer of ruthenium deposited on the electrode, that upon oxidative scans, converts into small RuO_2 particles with a very high surface area available for the water oxidation reaction. Environmental scanning electron microscopy analysis did not show the RuO_2 nanoparticles due to their small size, below the detection limit of the instrument. However, the nature of the catalyst have been thoroughly investigated using electrochemical and XAS techniques.[25] Despite the low catalyst loading, the activity of this GC-RuO_2 anode is very high at pH 7 as demonstrated by cyclic voltammetry experiments. The catalytic wave due to water oxidation shows a significant negative shift of the onset of the catalysis of *ca.* 250 mV compared to a platinum mesh electrode (Fig. 3a).

The performance of the GC-RuO_2 and SST-NiMoZn electrodes was tested independently by means of chronopotentiometry experiments in a three electrode configuration cell at pH 7. These experiments allowed us to simulate a real water splitting reaction that we would later do using the triple junction organic photovoltaic cell. We fixed the current at +405 μA and –405 μA for the GC-RuO_2 anode and SST-NiMoZn cathode respectively (red and pink traces, Fig. 3b). Analogous experiments were done for a platinum mesh anode and a platinum mesh cathode for comparison (green and black traces, Fig. 3b). All electrodes are stable under operating conditions, showing no loss of activity over the course of the experiment. It is interesting to see that the potential required for the water reduction reaction is exactly the same for both cathodes, the NiMoZn and Pt, accounting for less than 100 mV of overpotential, as had been previously reported in the literature.[26,27] On the other hand and consistent with the cyclic voltammetry experiments in Fig. 3a, the performance of the GC-RuO_2 is considerably superior

to that of platinum, which requires 250 mV more of potential than the former. Chronopotentiometry analysis of an ITO-CoPi[35,36,37,38] type electrode shows that our PV-EC system can also operate with such cobalt based anode, but with a ΔE *ca.* 100 mV higher than that of GC-RuO_2 and *ca.* 2000 times higher catalyst loading ($\Gamma \approx 0.30$ μmol cm^{-2}, Fig. S1). Thus, according to the chronopotentiometry experiments the voltage required to perform the water splitting reaction for the GC-RuO_2/SST-NiMoZn couple is ΔE = 1.78 V, which accounts for an overpotential of 550 mV. This value is *ca.* 250 mV lower than that observed for the Pt/Pt or Pt/SST-NiMoZn couples with ΔE = 2.03 (790 mV overpotential). The GC-RuO_2 anode not only minimizes the voltage at which the PV-EC device will operate, but also performs 9000 turnovers for a typical 1.5h experiment, accounting for an impressive TOF of 1.7 s^{-1}.

2.3-Bias-free water splitting catalysis with PV-EC cell at pH = 7

Water splitting experiments were performed illuminating a triple junction solar cell (η_{TJSC} = 8.2-8.7%) connected to a GC-RuO_2 anode and SST-NiMoZn cathode in a two electrode configuration setup in a pH 7 phosphate buffer solution (Fig. 4a). One of the advantages of this electrode combination is that both are highly selective, and back reactions are almost non-existent. However, a setup configuration in a two-compartment electrochemical cell separated by a glass frit was preferred, allowing for independent gas collection and avoiding potentially explosive gas mixtures. The current density versus time profile of a typical reaction is given in Fig. 4b. After an approximate 10 minutes stabilization time the current reaches a steady state at 4.5 mA/cm^2, and the operating potential remains at ΔE = 1.70-1.75 V for the whole duration of the experiment. This operating current density (J_{OP}) in mA/cm^2 can be used in

$$STH = \frac{J_{OP} \cdot 1.23 \cdot \eta_F}{P_{Solar}} \qquad (1)$$

where η_F is the Faradaic efficiency and P_{Solar} the power density, to determine the STH to be 5.6% under 1 sun AM 1.5G illumination. As shown in Fig 5 and using the full PV-EC system, continuous gas production was detected over a period of five hours with faradaic efficiencies close to 100% for both gases and no apparent loss of activity.

When performing the water splitting reactions we measured working voltages in the range of ΔE = 1.70-1.80 V, which closely matched the ΔE = 1.78 V and 1.76 V calculated from the chronopotentiometry experiments and the maximum power point of our triple junction solar cell, respectively (Fig. 2 and Fig. 3b). The minimum potential of 1.7 V measured at some instances with the triple junction cell relative to the chronopotentiometry measurement shown in Fig. 3b may correspond to slight differences in the RuO_2 layer coating the GC rod. The system is sensitive to high energy light as illustrated in Fig. S3. While an initial value of STH = 6.0% is obtained under full spectrum illumination, it decreases down to STH = 4.1% after 1.5 h. The cell degradation induced by the UV radiation can be eliminated by placing in front of the solar cell a 400 nm cut-off wavelength low band pass light filter. In that case we obtained stable profiles as can be seen in Fig. 4b and Supplementary Fig. S3. These STH values are amongst the highest reported in the literature for PV-EC hybrid devices that do not use silicon or group III-V semiconductors as light absorber, including two recently reported perovskite-$BiVO_4$ or perovskite-Fe_2O_3 tandem assemblies (STH = 2.5 % and 2.4 % respectively),[15,16] polymer solar cell (STH = 3.1-5.4 %)[18] or dye sensitized solar cell (STH = 3.1 %).[17] The parameters that allowed us to improve the latter reported benchmarking are: *i*) the high fill factor (76%) of the employed triple junction cell, as opposed to the 55-60% obtained for similar configurations[18b] and *ii*) the high performance of the GC-RuO_2 electorode at pH 7, that operates at sufficiently low overpotential. Both parameters are keys to minimize the efficiency loss during operating conditions. Other successful PV-EC examples include series connected PV cells based on either perovskite[14] or CIGS[10] semiconducting materials that provide the desired voltage and reach

STH higher than 10%. In these last two cases the conditions of the water splitting reaction are either strongly alkaline (1M NaOH) for the former or highly acidic (3M H_2SO_4) for the latter.

In the same conditions and configuration described in Fig. 4 we performed experiments simulating a more realistic scenario where long term stability is crucial for practical implementation. Water splitting was performed using a larger electrochemical cell to fit higher quantities of gases produced. After a 16 h illumination period the cells were kept in the dark for 8 h, after which time the experiment was resumed. The triple junction cell showed remarkable stability retaining 87 % of its initial efficiency after the first experiment and 82 % after the second one. A third cycle was performed accounting for a total illumination time of 50h and maintaining a 79 % of the efficiency (Fig. S3 in the supporting information). The changes in the shape of the j/E curve and its fill factor bring the optimal power point of the solar cell to lower potentials and decrease the overall efficiency of the system; since the water splitting reaction works at a constant potential in the range of 1.70-1.80 V, the current that passes through the system becomes lower. However, it is remarkable to see that at the end of the 50h illumination time all parameters still show 75% of their initial value or higher. To the best of our knowledge, this is one of the few examples that a PV-EC device, not containing silicon or a III-V semiconductor, shows such remarkable stability when tested for this time periods. Recent results demonstrate that under the proper fabrication procedure, encapsulation and adequate UV filtering solar cells based on PTB7 polymers are very stable and could improve the performance at long time experiments. Indeed, the backbone of the polymer does not show any degradation after more than 500 h under 1 sun continuous illumination.[28]

3-Conclusions

We have implemented a system where a 6% STH efficiency in the production of hydrogen is achieved at neutral pH. The system relies on a simple triple junction cell with an optimal light absorption and electrical performance. A cell FF as high as 76% allows for a water splitting reaction at a rate (current density) which is up to 96% the rate one would achieve if water splitting were to be carried out just above the thermodynamic potential threshold of 1.23V. In the triple junction studied the water splitting and the maximum power point are very close implying minimal electrical power losses. The catalysts used either for the oxidation or reduction part of the reaction use earth abundant materials or extremely small quantities of rare elements as Ru. To achieve a similar performance with the standard Pt electrodes one would have to raise the pH of the water solution to 14, otherwise at pH 7 the efficiency with such electrodes would remain close to just 3.5%. By anchoring Ru complexes on the surface of a glassy carbon rod, we have been able to reduce by several orders of magnitude the amount of RuO_2 needed with regard to previous anode configurations using that metal oxide. In such rod all the existing catalyst centers form a monolayer fully accessible to water molecules for oxidation, and the catalyst is highly active at pH 7. On the other hand, the electrical power is obtained from a PV cell based on a simple triple junction configuration where the three active layers are based on the same PTB7 polymer blend. PTB7 has been demonstrated to be one of the most efficient organic donor materials in photovoltaic cells. Additionally, PTB7 based cells are optimal for the development of a PV technology with a high potential for integration. Finally, recent work demonstrates that, contrary to results reported in prior studies, PTB7 based cells can be made very sable when the adequate cell fabrication procedure, encapsulation, and light filtering are applied.[28]

The system we report may ensure for the first time an eco-friendly large scale production of hydrogen from water at a neutral pH. The overall system is compact and has the potential to be fabricated at a low cost to effectively compete against other alternatives as hydrogen production

from methane where the cost is low but the environmental impact is large. Last but not least, PTB7 based cells can be made semi-transparent which makes them an optimal technology for the integration in the glass façades of city buildings where the electricity consumption is largest and where an infrastructure for natural gas distribution, which can be effectively utilized for the distribution of hydrogen, is already existing.

4-Experimental section

Materials. The PTB7 and PFN polymers from 1-Material, $PC_{71}BM$ (purity > 99%) from American Dye Source and ZnO nanoparticles (N-10, 6083, 2.5 wt% in isopropyl alcohol) from Nanograde were used as received. Photoactive material PTB7: $PC_{71}BM$ (1:1.5 wt %) were dissolved in chlorobenzene/1, 8-diiodoctane (97:3 vol %) mixture solvent, at a total concentration of 25 mg/mL. PFN was dissolved in methanol (1.0 mg mL^{-1}) in the presence of small amount of acetic acid (10 μL mL^{-1}), which was filtered with 0.45μm PTFE filter prior to use. ZnO solution was diluted with isopropyl alcohol (1:1, vol %) prior to use. The ZnO formulation is very stable and the performance would not drop even when left in air for more than one year. Ruthenium molecular precursor $[Ru(bda)(NO)(N\text{-}N_2)_2][PF_6]_3$ and the derivative GC-RuO_2 electrodes were prepared according to the literature, details about area and catalyst loading can be found in the supporting information.[24] The SST-NiMoZn cathodes were prepared following a modified procedure found in the literature, details found in the supporting information.[11]

Device fabrication and characterization. Triple junction devices were fabricated by spin-casting ZnO solution on the pre-cleaned ITO patterned glass substrates (Lumtec, 15 Ω/sq) and annealing at 120 ^{o}C in glovebox for 10 min to form a 20 nm condensed electron transporting layer. The active layer of the front sub-cell (~ 60 nm) was then spin-coated on the ZnO surface

and the films were dried under high vacuum (< 5 × 10^{-6} mbar) for one hour. Afterwards, interconnecting layer (ICL) of MoO_3 (10 nm, 0.5 Å /s)/ultrathin Ag (0.5 nm, 0.2 Å/s)/ PFN (10 nm) was deposited sequentially. Then, the active layer of the middle sub-cell (~ 105 nm) was spin-coated on the PFN surface, dried by vacuum for one hour. The second ICL was deposited using exactly the same procedure as the first one. The active layer of the rear sub-cell (~ 110 nm) was deposited on top of the second ICL and again left to dry in vacuum for 1 hour. Finally, MoO_3 (5 nm, 0.5 Å /s) and Ag (150 nm, 1 Å /s) electrodes were sequentially deposited through a shadow mask by thermal evaporation (< 5 × 10^{-6} mbar), which defines the device area of 9.0 mm^2. The triple-junction solar cells were encapsulated with glass slides using a UV-curable epoxy (ELC-4908, Electro-Lite Corp) in a N_2 glovebox before testing in ambient air. Current–voltage characteristics were measured under 1 sun AM 1.5G simulated sunlight (ABET Sol3A, 1000 W/m^2) with a Keithley 2420. The illumination intensity of the light source (Xenon lamp, 300W, USHIO) was determined using a Hamamatsu monocrystalline silicon reference cell calibrated by ISE Fraunhofer.

Supporting Information

Details about the equipment, materials and methods. Cathode and anode preparations. Additional chronopotentiometry and water splitting experiments. This material is available free of charge via the Internet at http://pubs.acs.org.

Acknowledgements: We acknowledge financial support from MINECO and the "Fondo Europeo de Desarrollo Regional" (FEDER) through grants MAT2014-52985-R, CTQ-2013–49075-R, SEV-2013-0319, and CTQ2014-52974-REDC. We also acknowledge financial support from the EU COST actions CM1202 and CM1205, and the EC FP7 Program (ICT-

2011.35) under grant agreement n° NMP3-SL-2013-604506. C.G.S. is grateful to AGAUR and GenCat for a “Beatriu de Pinós” postdoctoral grant. R.M thanks “La Caixa” Foundation for a PhD grant and Q.L acknowledges Erasmus Mundus doctorate program Europhotonics (Grant No. 159224-1-2009-1-FR-ERA MUNDUS-EMJD).

References

1. Betancur, R.; Romero-Gomez, P.; Martinez-Otero, A.; Elias, X.; Martorell J. *Nature Photonics* **2013**, 7, 995-1000.

2. Zhao, Y.; Meek, G. A.; Levine, B. G.; Lunt, R. R. *Adv. Opt. Mater.* **2014**, 2, 606-611.

3. Chen, Ch-Ch.; Dou, L.; Gao, J.; Chang, W-H.; Li, G.; Yang, Y. *Energy Environ. Sci.* **2013**, 6, 2714.

4. Walter, M. G.; Warren, E. L.; McKone, J. R.; Boettcher, S. W.; Mi, Q.; Santori, E. A.; Lewis N. S. *Chem. Rev.* **2010**, 110, 6446-6473.

5. Ager, J. W.; Shaner, M. R.; Walczak, K. A.; Sharp, I. D.; Ardo, S. *Energy Environ. Sci.*, **2015**, *8*, 2811-2824.

6. Khaselev, O.; Turner, J. A. *Science*, **1998**, 280, 425-427.

7. Khaselev, O.; Bansal, A.; Turner, J. A. *Int. J. Hydrogen Energy*, **2001**, 26, 127-132.

8. Licht, S.; Wang, B.; Mukerji, S.; Soga, T.; Umeno, M.; Tributsch *H. Int. J. Hydrogen Energy* **2001**, 26, 653.

9. Cox, C. R.; Lee, J. Z.; Nocera, D. G.; Buonassisi, T. *Proc. Natl. Acad. Sci. U.S.A.* **2014**, 111, 14057-14061.

10. Jacobsson, T. J.; Fjällström, V.; Sahlberg, M.; Edoff, M.; Edvinsson, T. *Energy Environ. Sci.* **2013**, 6, 3676-3683.

11. Reece, S. Y.; Hamel, J. A.; Sung, K.; Jarvi, T. D.; Esswein, A. J.; Pijpers, J. J. H.; Nocera, D. G. *Science* **2011,** *334,* 645.

12. Vito, C.; Berardi, S.; Caramori, S.; Argazzi, R.; Carli, S.; Meda, L.; Tacca, A.; Bignozzi, C. *Phys. Chem. Chem. Phys* **2013,** *15,* 13083.

13. Han, L.; Abdi, F. F.; van de Krol, R.; Liu, R.; Huang, Z.; Lewerenz, J.; Dam, B.; Zeman, M.; Smets, A. H. M. *Chem. Sus. Chem*. **2014**, 7, 2832-2838.

14. Luo, J.; Im, J-H.; Mayer, M. T.; Schreier, M.; Nazeeruddin, M. K.; Park, N-G.; Tilley, S. D.; Fan, H. J.; Grätzel, M. *Science* **2014,** *345,* 1593.

15. Chen, Y-S.; Manser, J. S.; Kamat, P. V. *J. Am. Chem. Soc.* **2015**, 137, 974-981.

16. Gurudayal, S. D.; Kumar, M. H.; Wong, L. H.; Barber, J.; Grätzel, M.; Mathews, N. *Nano Lett.* **2015**, 15, 3833-3839.

17. Brillet, J.; Yum, J-H.; Cornuz, M.; Hisatomi, T.; Solarska, R.; Augustynsky, J.; Grätzel, M. *Nature Photonics* **2012,** *6,* 824.

18. a) Shi, X.; Zhang, K.: Shin, K.; Ma, M.; Kwon, J.; Choi, I. T.; Kim, J. K.; Kim, H. K.; Wang, D. H.; Park, J. H. *Nano Energy*, **2015**, 13, 182. b) Esiner, S.; Willems, R. E. M.; Furlan, A.; Li, W.; Wienk, M. M.; Janssen, R. A. *J. Mat. Chem A* **2015**, 3, 23936-23945.

19. Esiner, S.; Van Eersel, H.; Wienk, M. M.; Janssen, R. A. J. *Adv. Mater.*, **2013**, 25, 2932-2936.

20. McCrory, C. C. L.; Jung, S.; Ferrer, I. M.; Chatman, S. M.; Peters, J.; Jaramillo, T. F. *J. Am. Chem. Soc.* **2015**, 137, 4347.

21. Tsuji, E.; Imanishi, A.; Fukui, K.-I.; Nakato, Y. *Electrochimica Acta.* **2011**, 56, 2009-2016.

22. Licht, S.; Wang, B.; Mukerji, S. *J. Phys. Chem. B* **2000**, 104, 8920-8924.

23. Spurgeon, J.; Velazquez, J. M.; McDowell, M. T. *Phys. Chem. Chem. Phys*. **2014**, *16*, 3623-3631.

24. Duan, L.; Bozoglian, F.; Mandal, S.; Stewart, B.; Privalov, T.; Llobet, A.; Sun, L. *Nature Chem.* **2012**, 4, 418-423.

25. Matheu, R.; Francàs, L.; Chernev, P.; Ertem, M. Z.; Batista, V.; Haumann, M.; Sala, X.; Llobet, A. *ACS Catalysis*. **2015**, 5, 3422.

26. Stachurski, J. Z. O.; Williamsville, D. P.; Ripa, J. A.; Pokrzyk, G. F. *U. S. Patent* **1982**, 4,354,915.

27. Nocera, D. G. *Acc. Chem. Res.* **2012**, *45*, 767-776.

28. Liu, Q.; Mantilla-Perez, P.; Montes Bajo, M.; Romero-Gomez, P.: Martorell, J. *to be published*.

29. Li, G.; Zhu, R.; Yang, Y. *Nature Photon.* **2012**, 6, 153-161.

30. Bahro, D.; Koppitz, M.; Mertens, A.; Glaser, K.; Mescher, J.; Colsmann, A. *Adv. Energy Mater.* **2015** *DOI: 10.1002/aenm.201501019*.

31. Martínez-Otero, A.; Liu, Q.; Mantilla-Perez, P.; Montes Bajo, M.; Martorell, J. *J. Mater. Chem. A* **2015**, 3, 10681-10686.

32. Mantilla-Perez, P.; Martínez-Otero, A.; Romero-Gomez, P.; Martorell, J. *ACS Appl. Mater. Interfaces* **2015**, 7, 18435-18400.

33. Martínez-Otero, A.; Elias, X.; Betancur, R.; Martorell, J. *Adv. Optical Mater*. **2013**, 1, 37-42.

34. Urbain, F.; Smirnov, V.; Becker, J-P.; Lambertz, A.; Rau, U.; Finger, F. *Sol. Energ. Mater. Sol. Cells* **2016**, 145, 142–147.

35. Kanan, M. W.; Nocera, D. G. *Science* **2008**, 321, 1072-1075.

36. Lutterman, D. A.; Surendranath, Y.; Nocera, D. G. *J. Am. Chem. Soc.* **2009**, 131, 3838-3839.

37. Esswein, A. J.; Surendranath, Y.; Reece, S. Y.; Nocera, D. G. *Energy Environ. Sci.* **2011**, 4, 499-504.

38. Zhong, D. K.; Choi, S.; Gamelin, D. R. *J. Am. Chem. Soc.* **2011**, 133, 18370-18377.

Figures

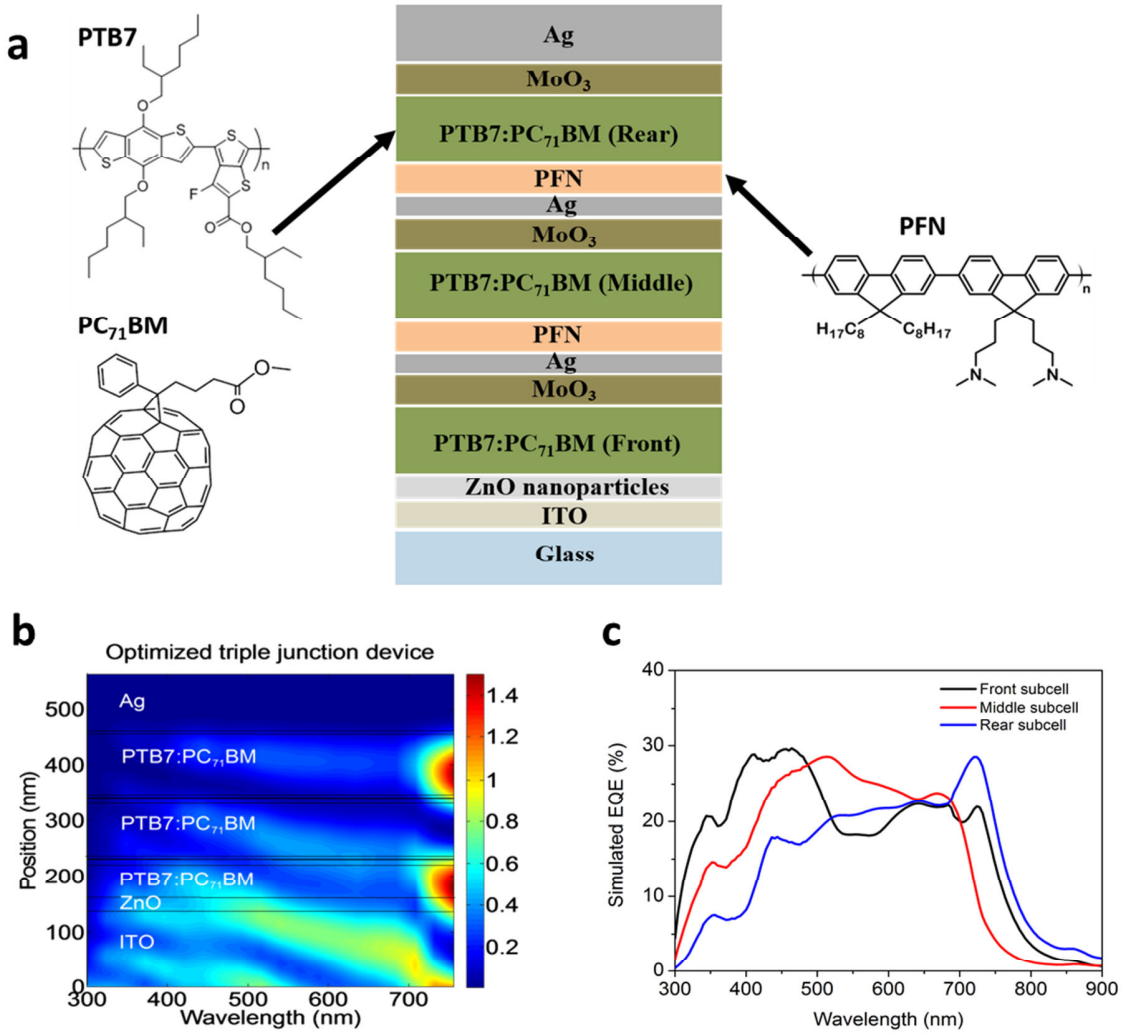

Figure 1 Optically optimal triple junction cell **a)** Schematic representation of the triple junction solar cells and molecular structure of its organic polymers. PTB7, Poly({4,8-bis[(2-ethylhexyl)oxy]benzo[1,2-b:4,5-b′]dithiophene-2,6-diyl}{3-fluoro-2-[(2-ethylhexyl)carbonyl]thieno[3,4-b]thiophenediyl}. $PC_{71}BM$, [6, 6]-phenyl-C_{71} butyric acid methyl ester. PFN, poly [(9,9-bis(3'-(N,N-dimethylamino)propyl)-2,7-fluorene)-alt-2,7-(9,9–

dioctylfluorene. **b)** Calculated electrical field intensity normalized with respect to the incident field intensity as a function of wavelength for an optimized triple junction organic solar cell architecture. **c)** Calculated EQE for each one of the three sub-cells in an optimized architecture.

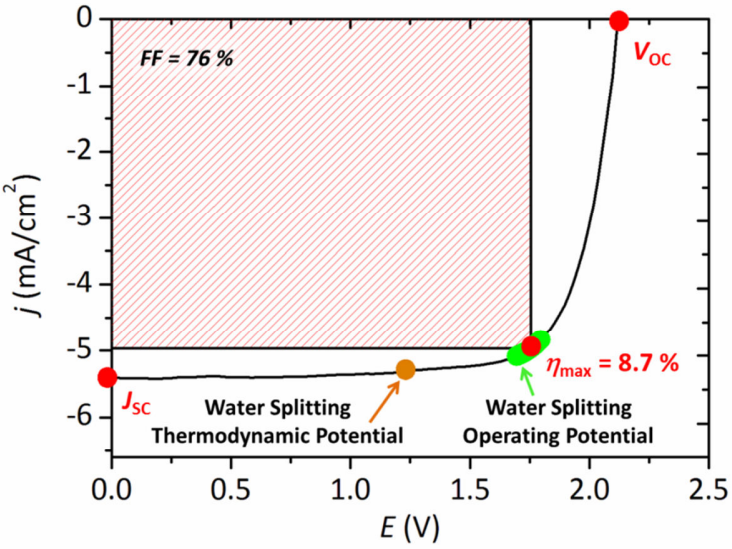

Figure 2. *j*/*E* curve of triple junction cell. V_{OC} = 2.13 V, J_{SC} = 5.4 mA/cm^2, FF = 76% and η_{max} = 8.7% where the water splitting thermodynamic potential (orange) and water splitting operating potential range (green) are indicated. V_{OC}: open circuit potential, J_{SC}: short circuit current density, FF: fill factor and η_{max} = cell efficiency at maximum power point.

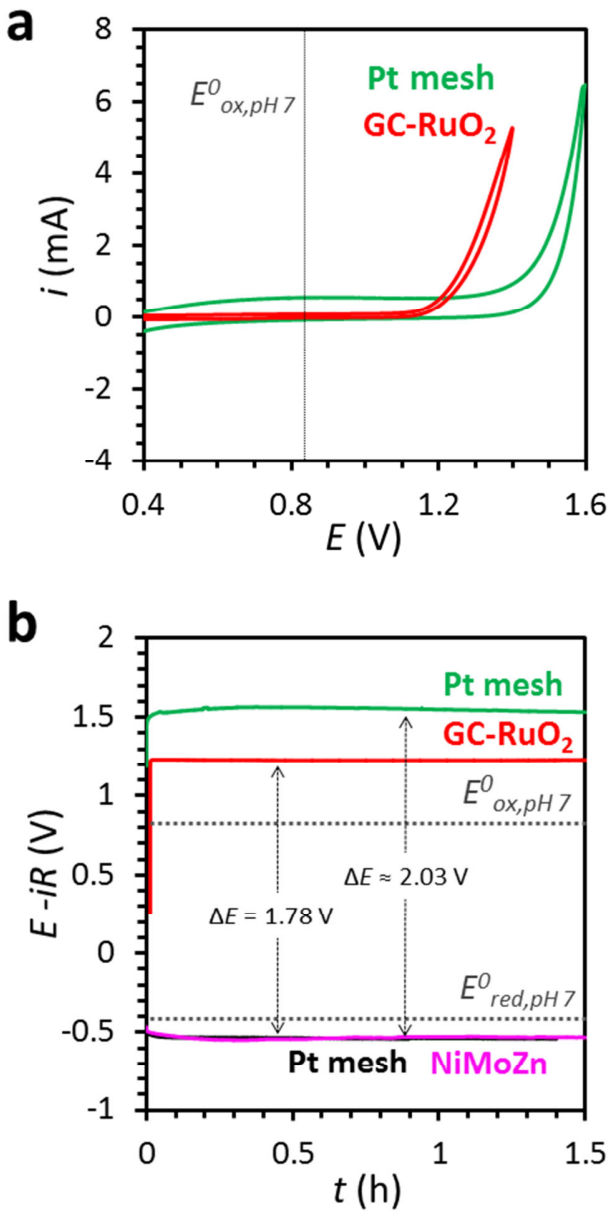

Figure 3. a) Cyclic voltammetry experiments of a GC-RuO_2 (red) and platinum mesh (green) working electrodes. **b)** Chronopotentiometry experiments at a fixed current of +405 µA for GC-RuO_2 (red) and Pt mesh (green) or –405 µA for NiMoZn (pink) and Pt mesh (black). All experiments in a) and b) were done in a two compartment cell, in degased 0.1 M phosphate buffer, at pH 7.0, using a platinum mesh as counter electrode and Ag/AgCl as reference electrode. The potentials are given against the NHE reference electrode using the conversion $E_{NHE} = E_{Ag/AgCl} + 0.2$. The thermodynamic potentials for the water oxidation (E^0_{ox}, pH 7 = 0.817 V) and water reduction (E^0_{red}, pH 7 = –0.413 V) reactions at pH 7 are indicated in grey dotted lines.

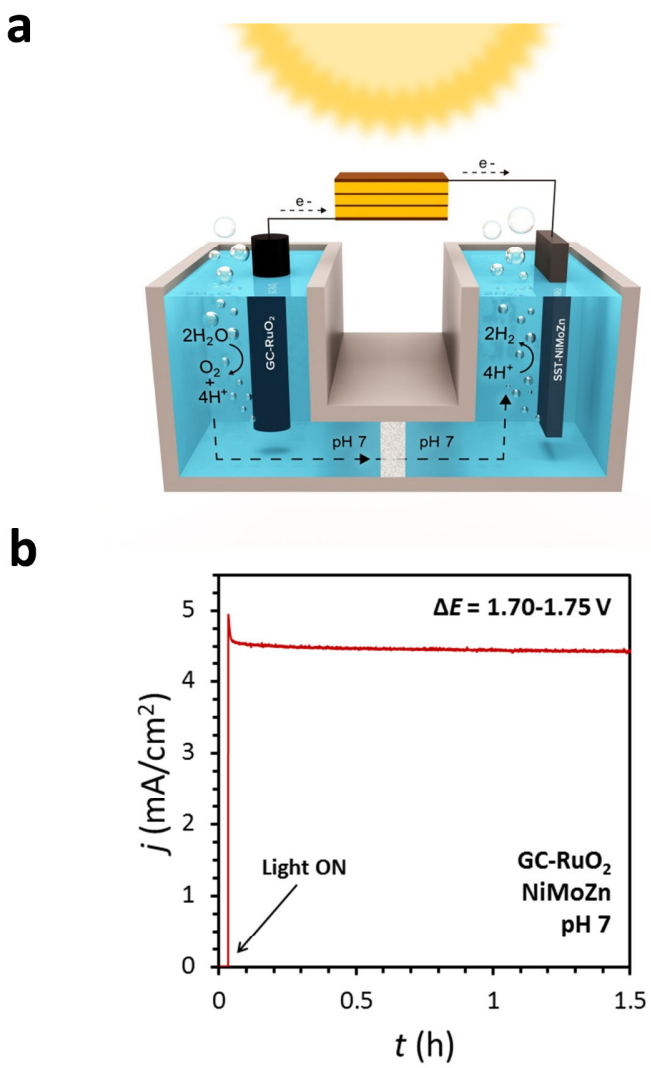

Figure 4. Water splitting EC-PV system **a)** Schematic representation of the setup for the water splitting experiments using a triple junction organic solar cell, GC-RuO_2 anode and SST-NiMoZn cathode. **b)** Current *vs* time profile of a water splitting experiment using a triple junction solar cell (η_{TJSC} = 8.5 %), GC-RuO_2 anode and SST-NiMoZn cathode in a two electrode configuration and a two compartment cell containing 0.1 M phosphate buffer, pH = 7.0, under AM 1.5 G illumination with a GG400 filter. The operating potential of the reaction was measured manually and is also indicated. After 1.5 h, the amount of evolved gas accounted for TON_{Ru} = 9 000 and TOF = 1.7 s^{-1}, where TON_{Ru} = mols O_2/mols of Ru and TOF = mols O_2/(mols of Ru×second).

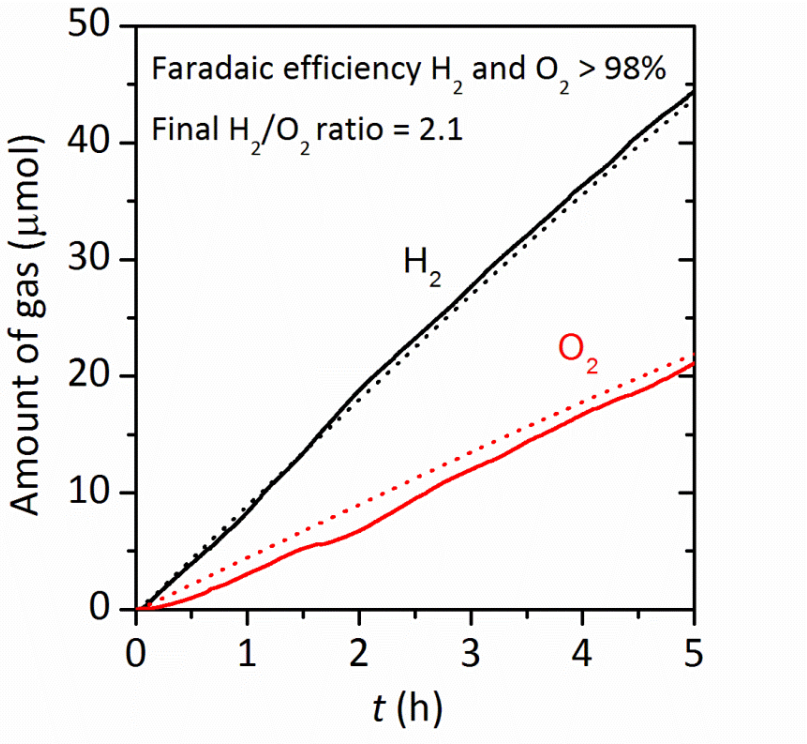

Figure 5. Gas evolution of a water splitting experiment using a triple junction solar cell (η_{TJSC} = 8.2%), GC-RuO_2 anode and SST-NiMoZn cathode in a two electrode configuration and a two-compartment cell, containing 0.1M phosphate buffer, pH = 7, under 1 sun irradiation (λ > 400 nm). The dotted lines represent the 100% faradaic efficiency based on the charge passed during electrolysis while the solid lines represent the gas measured with Clark electrode sensors.

Table of Contents and Abstract Graphic

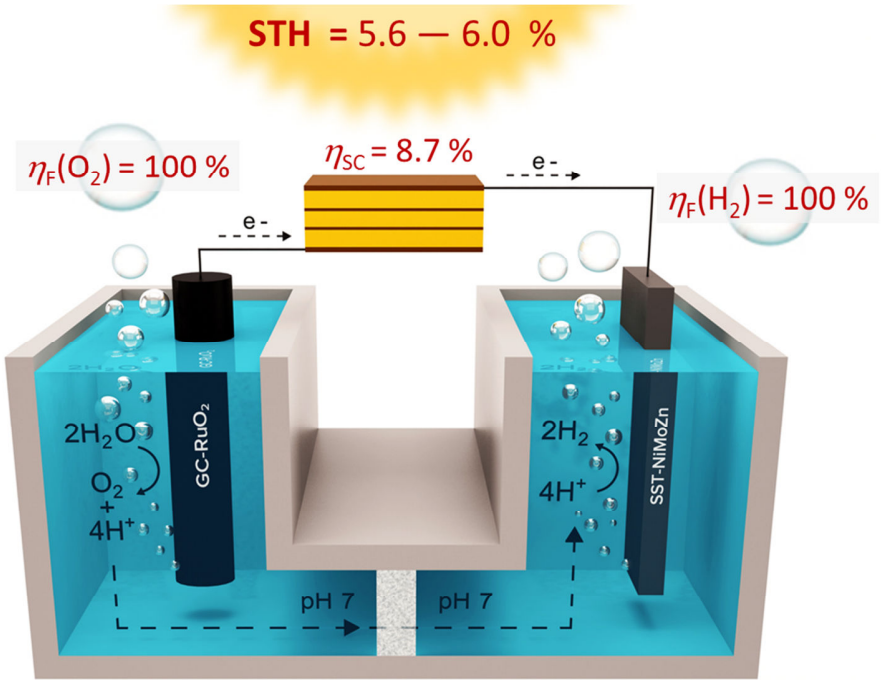

ToC Text:

Efficient visible light induced hydrogen production from water at neutral pH, using a simple triple junction cell coupled to a RuO_2 anode and a NiMoZn cathode, reaching 6% STH.